Langmuir

ARTICLE

pubs.acs.org/Langmuir

Kinetics Study of Crystallization with the Disorder−bcc−fcc Phase Transition of Charged Colloidal Dispersions

Hongwei Zhou,[†,‡] Shenghua Xu,[†,‡] Zhiwei Sun,[*,†,‡] Xuan Du,[†,‡] and Lixia Liu[†,‡]

[†]Key Laboratory of Microgravity and [‡]National Microgravity Laboratory, Institute of Mechanics, Chinese Academy of Sciences, No. 15 Beisihuanxi Road, Beijing 100190, People's Republic of China

ABSTRACT: Structure transformation (disorder−bcc−fcc) in charged colloidal dispersions, as a manifestation of the Ostwald's step rule, was confirmed by means of reflection spectrum (RS) measurements in our previous study. By taking advantage of a reflection spectrum containing plenty of information about the crystallization behaviors, time-dependent changes of parameters associated with the crystal structure and composition during the disorder-bcc-fcc transition are reported by treating the data from RS in this article. In addition, Avrami's model is adopted to analyze the transition process and investigate the transition rate. On the basis of the above investigations, associated kinetic features of crystallization with the disorder-bcc-fcc transition are described.

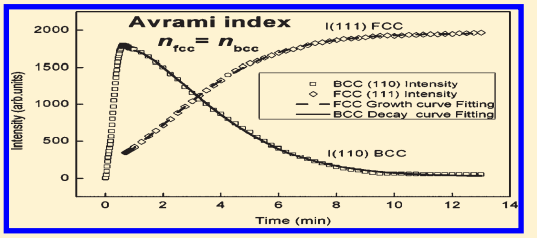

INTRODUCTION

Charged colloidal particles dispersed in deionized water under certain conditions can be self-assembled into highly ordered arrays of particles: colloidal crystals. This self-assembly process of colloids is analogous to their atomic or molecular counterparts. Because time and length scales in colloidal crystals are several orders of magnitude larger than those in atomic or molecular crystals, more suitable tools and instruments, such as microscopy and a light-scattering method, can be acquired for observation and measurement in the investigation of crystallization. Therefore, colloidal crystals provide an important model system for studying the general principles of the crystallization of materials.[1−9]

Understanding the mechanisms underlying the transition dynamics of colloidal crystallization is of fundamental importance in assessing the validity of classical crystal growth theories and in controlling the crystal morphology. For example, the validity of Ostwald's step rule, as an empirical rule, has long been a widely investigated issue in science and technology. An acknowledged theoretical basis for the step rule has not been formulated, although laboratory observations supporting the rule are now innumerable with only rare exceptions. Related to the step rule, Alexander and McTague[10] further predicted that a bcc structure appears first regardless of whether a thermodynamically more stable one exists. As a model system, it is desirable to see whether the colloidal crystallization obeys Ostwald's step rule.[1,11] In this regard, the phenomenon that, in some cases, the bcc structure appeared first before the fcc phase was formed during the crystallization of charged colloidal particles was observed.[12] Some computer simulations,[13,14] including our Brownian dynamics simulation,[15] have also demonstrated the bcc−fcc structural transition. With the aid of a reflection spectrometer, our previous study provided direct evidence of the existence of a transition from the bcc to the fcc phase by quantitatively confirming the growth of the fcc structure at the expense of the bcc structure. We further showed that the lifetime of the bcc metastable structure in this system depended significantly on the particle volume fraction.[16]

Actually, the changes in the crystal structure and composition with time during the crystallization may provide valuable clues to gaining insight into the kinetics of the nucleation and growth of crystals. In general, the relevant parameters, such as crystallinity, number of crystallites, and average crystal size[17−20] may change considerably during the crystallization. Commonly, however, the structures of colloidal crystals are considered to be unchanged during crystallization, and many existing studies concern only the above-mentioned parameters corresponding to one crystal structure. As a matter of fact, polymorphism and polymorphic transformation are also quite common for atomic and molecular crystals.[21−28] Therefore, it is worthwhile to study the crystallization process accompanied by structure transitions for colloidal crystals as a model system of atomic and molecular crystals.

When the bcc metastable structure appears during the transition from the liquid (disordered) state to the equilibrium fcc structure, significant changes in the above-mentioned parameters are expected. A reflection spectrum contains plenty of information about the crystallization kinetics.[29−31] How to understand and interpret the spectrum is the key to extracting the required information from the spectrum measurements. In an effort to explore the kinetics involved in this disorder−bcc−fcc transition, the focus of this article is on the evolution tendency of these parameters achieved from time-resolved reflection spectrum measurements. The transformation rate is evaluated, and the evolution of crystallinity, the average crystal size, and the

Received: January 31, 2011
Revised: April 18, 2011
Published: May 20, 2011

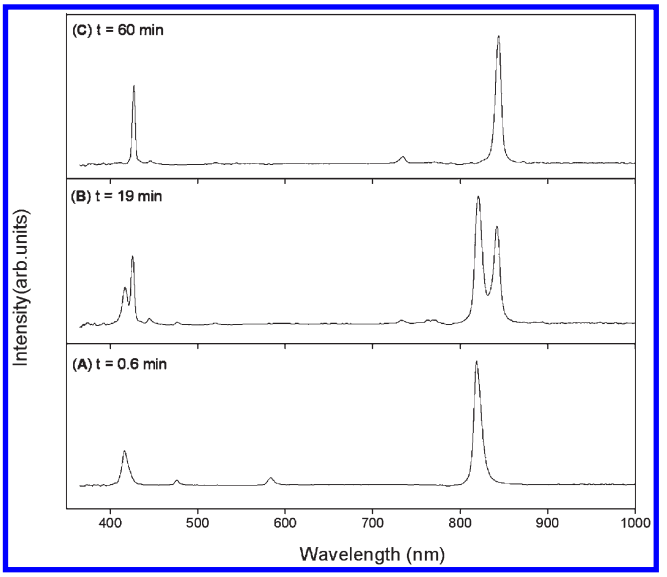

Figure 1. Reflection spectra of the latex solution (Φ = 0.75%) at different intervals after the cessation of shear. (A) 0.6 min. (B) 19 min. (C) 60 min.

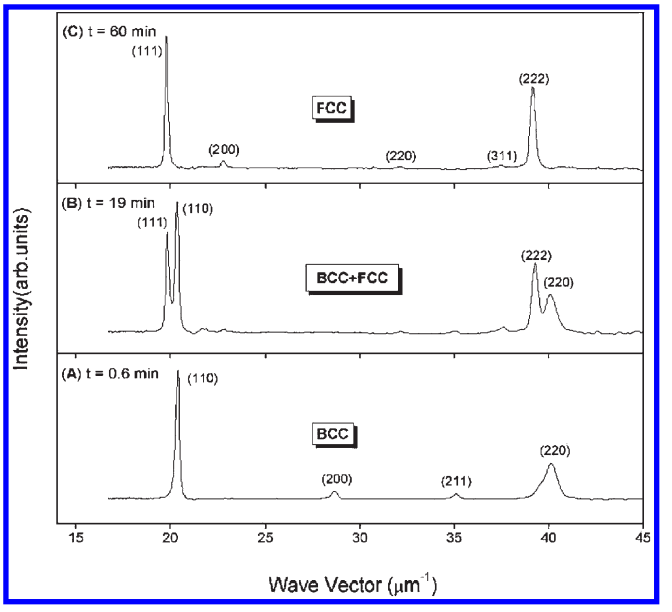

Figure 2. Converted Bragg scattering intensity distribution at different wave vectors (Φ = 0.75%). (A) 0.6 min bcc lattice. (B) 19 min. Coexistence of bcc and fcc lattices. (C) 60 min fcc lattice.

number of crystals during the transformation are discussed. In addition, the experimental results for different volume fractions are compared to study the influence of volume fraction on crystallization.

EXPERIMENTAL SECTION

Materials and Sample Preparation. The negatively charged polystyrene (PS) particles used in this study were synthesized by an emulsion polymerization method.[32] Thereafter, purification of the spheres was performed by filtration and followed by repeated washing with fresh distilled water in the centrifugation process. The latex was stored with resin (AG501-X8(D), Bio-Rad Laboratories, USA) for further use. The mean diameter and polydispersity of the particles determined by dynamic light scattering are 101 nm and 4%, respectively. The analytical charge density is 9.9 $\mu C \cdot cm^{-2}$ according to conductometric titration. The samples used in this study were prepared by carefully mixing the as-prepared latex with a certain amount of pure water, and then the mixtures were sonicated for several minutes to attain homogeneous ones.

Experimental Setup. The experimental setup used in this study is the same as that described in our previous paper.[33] This system included a suspension circulation system that consisted mainly of a crystallization cell, a reflection spectrometer, a circulating pump, an ion-exchange chamber, and a conductivity measurement unit. A fiberoptic spectrometer (Avaspec-2048, Avantes, Netherlands) with a tungsten halogen light source (Avalight-HAL, Avantes, Netherlands) and a bifurcated fiber optic cable were used to scan the light intensity reflected from the crystallization cell over a certain wavelength range. The fast data collection rate of the reflection spectrum made it possible to trace the light intensity changes in the structure transformation process.

RESULTS AND DISCUSSION

Our previous study has shown that the RS method can also determine the crystal structure.[33] An example is shown in Figures 1 and 2 in which the volume fraction is 0.75%. The reflection spectra show the intensity distribution at different wavelengths, as seen in Figure 1. Because wave vector can be written as $q = (4\pi\nu/\lambda)\sin(\theta/2)$, where ν is the refractive index of the suspension medium, λ is the vacuum wavelength, and θ is the scattering angle (θ = 180° in this study), the reflection spectra can be converted to that in the wave vector space, as shown in Figure 2. By analyzing the relative positions of the diffraction peaks originating from different crystal planes, the crystal structure can be determined quickly using the reflection spectrum. In this study, all of the analyses will be based on the reflection spectra in the wave vector space.

We have shown that fcc is the equilibrium phase for volume fractions larger than 0.57%.[16] To ensure that the transition is away from the bcc−fcc boundary (around which the transformation is very time-consuming), the volume fractions adopted in this study are 0.75 and 0.92%. Figure 2 clearly shows the structural evolution from bcc to fcc in the crystallization of the sample with a volume fraction of 0.75%. In Figure 2A, the wave vectors corresponding to these peaks are 20.4, 28.6, 35.1, and 40.1 μm^{-1} and the ratio is $\sqrt{2}/\sqrt{4}/\sqrt{6}/\sqrt{8}$, so the crystal structure is bcc. In Figure 2C, the wave vectors are 19.8, 22.8, 32.1, 37.5, and 39.2 μm^{-1} and the ratio is $\sqrt{3}/\sqrt{4}/\sqrt{8}/\sqrt{11}/\sqrt{12}$ so that the crystal structure is fcc. Such a structure evolution also appears for a volume fraction of 0.92%. Therefore, crystallization with the disorder−bcc−fcc transition can be studied by analyzing the corresponding reflection spectra in the wave vector space for these samples. It should be noticed that R_{exp} (Bragg spacing, calculated from the position of the primary peak) is always smaller than R_0 (average spacing, calculated from the volume fraction and diameter of the particles) for both samples, which implies the coexistence of voids (rare phase) and ordered crystallites (dense phase).[34] The result $R_{exp} < R_0$ happens to coincide with the assumption that there may be attractive interparticle interactions, as assumed by Ise et al.[4] This result is consistent with studies by other researchers in which the properties were studied by methods based on Bragg diffraction such as SLS (static light scattering) and USAXS (ultra-small-angle X-ray scattering).[34−37]

Commonly, the crystallization processes are studied from the evolution of the primary peak.[29] When there is only one structure in

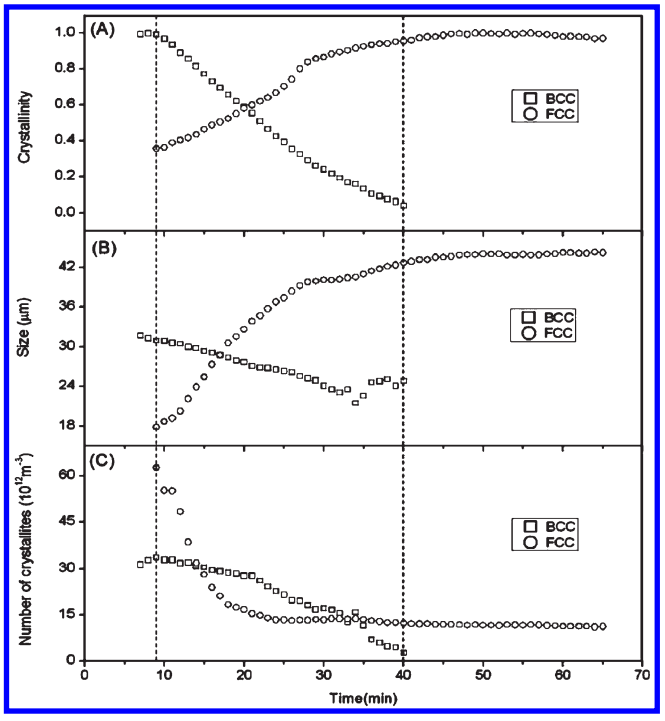

Figure 3. Relevant parameter changes in the structure-transformation process. Dashed vertical lines in the graph indicate the start time and end time (Φ = 0.75%). (A) Crystallinity. (B) Average crystal size. (C) Number of crystallites.

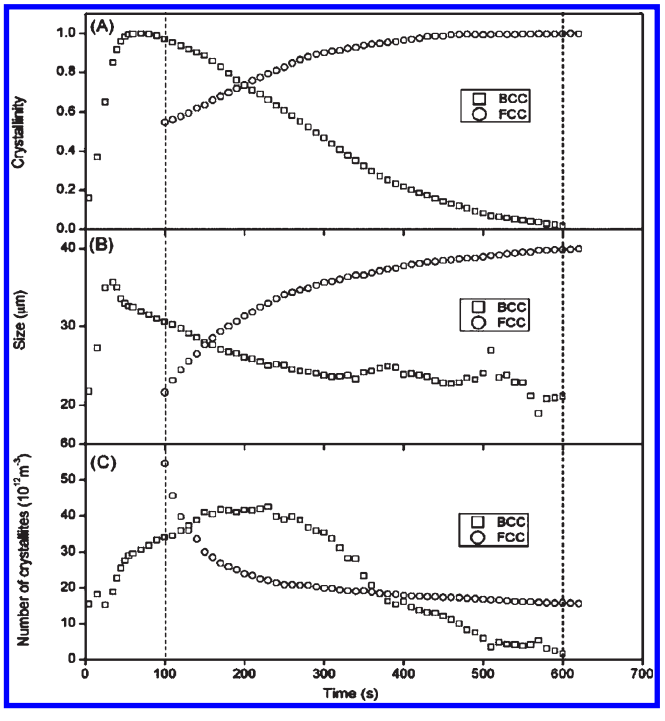

Figure 4. Relevant parameters changes in the structure transformation process. Dashed vertical lines in the graph indicate the start time and end time (Φ = 0.92%). (A) Crystallinity. (B) Average crystal size. (C) Number of crystallites.

the system, the primary peak will be far from the other-higher order diffraction peaks, as shown in Figure 2A,C. However, during the transition process, the coexistence of bcc and fcc structure may cause their corresponding primary peaks to be very close and overlap with each other, forming an indistinguishable peak, as seen in Figure 2B. To separate fcc and bcc peaks, we assume that each of them has an approximately Gaussian-shaped distribution centered at $q(111)$ and $q(110)$ for fcc and bcc structures, respectively. In this way, the evolution of the primary peaks of bcc and fcc can be individually treated.

Some important parameters such as crystallinity $X(t)$, the average crystal size $L(t)$, and the number of crystallites $N_c(t)$ are helpful in studying the crystallization kinetics and in characterizing the crystallization process. For the SLS method, these parameters can be evaluated from the Bragg peaks.[17−20,38−40] Our previous study[33] has compared the SLS method with our (RS) method, which is also used in this study, showing that both methods share the same principle as long as the profile of RS is transferred from the wavelength space to the wave vector space. Therefore, to evaluate the above parameters from the Bragg peaks measured by RS (in wave vector space), exactly the same analysis method used in SLS can be applied. From the separated peaks of the bcc (110) and fcc (111) planes, we can calculate the values of $A(t)$ (integrated area of the peak), $\Delta q(t)$ (full width at half-maximum of the peak), and q_{hkl} (position of the peak), respectively. Then the above parameters can be evaluated as follows:

(1) The crystallinity $X(t)$ represents the fraction of the sample that becomes the part of crystallites. When all of the liquid is converted to the crystal state, the crystallinity is 1. $X(t)$ is calculated from peak area $A(t)$ by

$$X(t) = cA(t) \quad (1)$$

where c is the normalization factor. The normalization factor for bcc is based on the maximum value of the peak area of the bcc (110) plane during crystallization, and the normalization factor for fcc is based on the maximum value of the peak area of the fcc (111) plane in the equilibrium phase.

(2) The average crystallites size $L(t)$ can be calculated from the width of the Bragg peaks.[17−20,38−40] It is given by

$$L(t) = \frac{2\pi K}{\Delta q(t)} \quad (2)$$

where K = 1.155 is the Scherrer constant for a crystal of cubic shape.[38−40]

(3) The number density of the crystallites, N_c, is estimated by

$$N_c(t) = \frac{X(t)}{L^3(t)} \quad (3)$$

(4) The lattice constant (l) and the smallest interparticle distance (D) can be deduced from the primary peak center wave vector (q) of bcc and fcc by the following equations:

$$l_{bcc} = \frac{2\pi}{q_{bcc}} \times \sqrt{2},\ l_{fcc} = \frac{2\pi}{q_{fcc}} \times \sqrt{3} \quad (4)$$

$$D_{bcc} = \frac{\sqrt{6}\pi}{q_{bcc}},\ D_{fcc} = \frac{\sqrt{6}\pi}{q_{fcc}} \quad (5)$$

The results of crystallinity, the average crystallites size, and the number density of crystallites for volume fractions of

dx.doi.org/10.1021/la200407h |*Langmuir* 2011, 27, 7439–7445

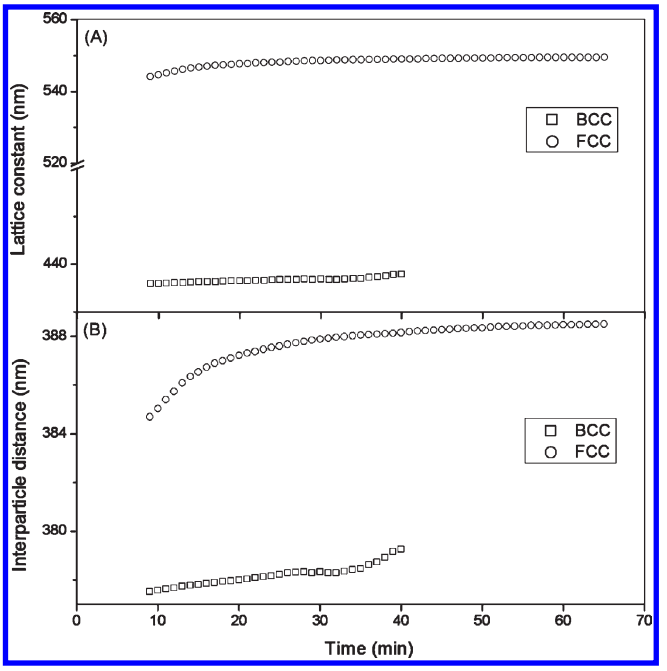

Figure 5. Changing tendencies of (A) the lattice constant and (B) the interparticle distance in the transition process (Φ = 0.75%).

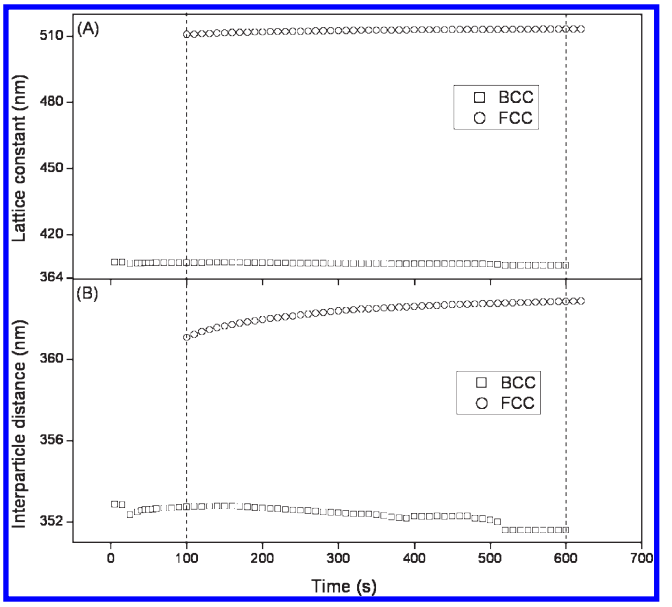

Figure 6. Changing tendencies of (A) the lattice constant and (B) the interparticle distance in the transition process (Φ = 0.92%).

0.75 and 0.92% are shown in Figures 3 and 4, respectively. Our main interests here are to study the transition process, which is indicated by two dashed line in the picture. The left dashed line indicates the time from which the bcc (110) and fcc (111) peaks can be distinguished, the right dashed line indicates the time from which metastable bcc disappears completely and the part between the two dashed lines indicates the coexistence of bcc and fcc structures. In Figures 3 and 4, only fcc exists on the right side of the right dashed line, so the relevant values of the *b*cc are omitted. Similarly, only the growth of metastable bcc in the early stage of crystallization (left side of the left dashed lines) has been shown in these Figures. During this time, only bcc exists, so the relevant values of fcc are omitted.

The Figures of all parameters show obvious similarity in the changing tendencies for the two volume fractions. The major difference is the duration time of the bcc−fcc transformation, which is much longer for a volume fraction of 0.75% (about 30 min) than for a volume fraction of 0.92% (about 8 min). Both Figures 3 and 4 show that the crystallinity of bcc first increases very fast and then decreases with the increase in the crystallinity of the fcc structure. Finally, the $X(t)$ of bcc approaches zero, and that of fcc reaches a maximum value. These results confirm that bcc is a metastable structure and will transform to a stable fcc structure.

Starting from the onset of the transition (indicated by the left dashed line), the crystallinity of bcc is decreasing and that of fcc is increasing, as shown in Figures 3A and 4A. The variation of the average crystal size is similar to the change in crystallinity, as seen in Figures 3B and 4B. The number of fcc crystallites decreases quickly after the start of the transition process and then it changes very slowly, and the number of bcc crystallites may increase a little before decreasing, which can be seen in Figure 4C.

The relevant changes in these parameters as shown in Figures 3 and 4 can help us understand the crystallization process. At the beginning of the crystallization, most colloidal particles transform quickly from an initial liquid state to a metastable bcc state. Soon after, the metastable bcc state begins to transform into a stable fcc state. From the onset of the transformation, the size of the bcc crystals begins to decrease because more and more particles join in the formation of fcc structures. The above data suggest a possible process for the transition described below: at the beginning of the transition, some bcc crystals break into smaller pieces so that the number of bcc crystals increase for a while as shown in Figure 4C. For fcc crystals, the size is always increasing and the number of crystallites keeps decreasing. In the early stage of the transition, a quickly increasing crystal size and a quickly decreasing number of crystallites imply that some fcc crystals may coalesce to form larger crystals. Finally, the crystallinity $X(t)$ and the number of bcc crystals drop to zero, indicating that all bcc crystals transformed into fcc crystals.

Structural parameters such as the lattice constant and interparticle distance characterizing the lattice site are also important for a better understanding of the crystal's microstructure in the transformation process. Their evolutions are shown in Figures 5 (Φ = 0.75%) and 6 (Φ = 0.92%). Unlike the changes in crystallinity, the values of the lattice constant and interparticle distance remain almost constant during the whole transformation process.

Combining the above pieces of information about the variation of parameters, including the crystallinity, average crystal size, number of crystallites, lattice constant, and shortest interparticle distance, we can draw a brief picture of the crystallization kinetics and the structure-transformation process. First, metastable bcc structures form quickly, and then negligibly small "droplets" of the stable fcc nucleate from the metastable background along with the cleavage of bcc pieces. The particles near the boundary of bcc crystals maybe gradually roam away from the ordered region of bcc and migrate to the growing grains of fcc. The ordered grains of bcc keep shrinking until all of the particles are assimilated by the growing grains of fcc. Meanwhile, some of the growing fcc grains may coalesce. At last, these fcc grains grow further to form larger crystals.

It is well known that Avrami's law or the Kolmogorov−Johnson−Mehl−Avrami (KJMA) approximation[41−43] has been

dx.doi.org/10.1021/la200407h |*Langmuir* 2011, 27, 7439–7445

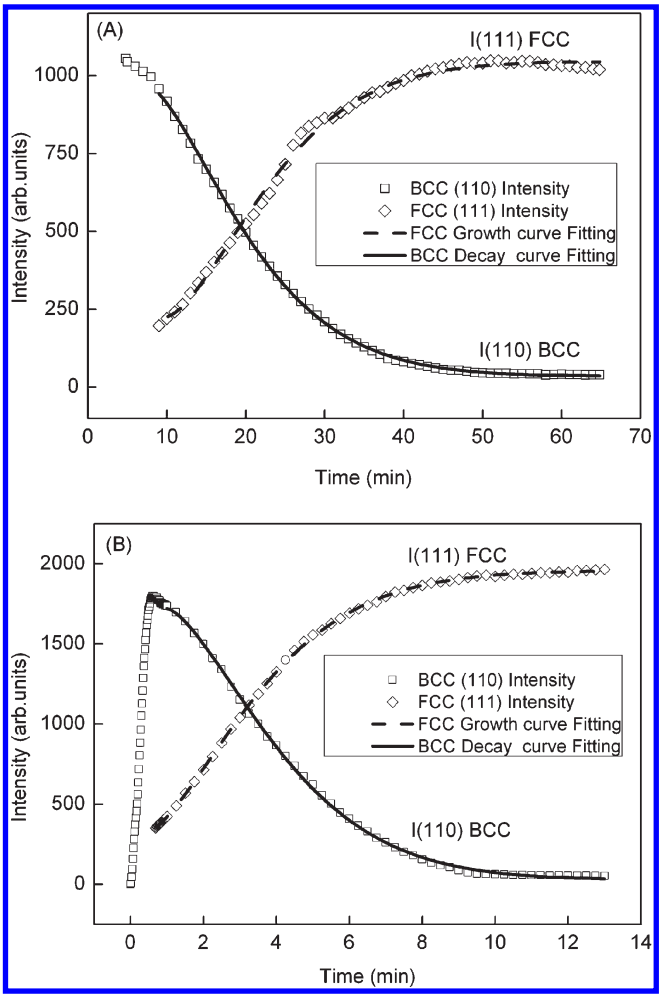

Figure 7. Intensity changes of bcc (110) and fcc (111) during structure evolution. Avrami's model for the kinetics of nucleation and growth was used for curve fitting. The solid line and dashed line are best-fit results of the peak intensity of bcc (110) and fcc (111), respectively. (A) $\Phi = 0.75\%$. (B) $\Phi = 0.92\%$.

widely used to analyze order−order transitions and metastable decay in fields ranging from metallurgy[44−46] to polymer science.[47−49] More generally, for systems with a nonconserved order parameter in which the decay is driven by a difference between the free-energy densities of the metastable and equilibrium phases, Avrami's model should be applicable.[50]

In this study, Avrami's model is adopted to analyze the transition process. Assuming that the intensities are proportional to the amount of transformed material,[51] the kinetics of the structure-evolution process can be analyzed by tracking the intensity changes of the two independent peaks. The intensity changes of peaks corresponding to the bcc (110) plane and the fcc (111) plane are shown in Figure 7. In Figure 7A, the volume fraction is 0.75%, and in Figure 7B, the volume fraction is 0.92%. We should mention that for 0.92%, a faster sampling rate is utilized and the growth of metastable bcc is also exhibited. Clearly, both transitions for the two volume fractions show that the peak intensity of bcc decreases to almost zero and that of fcc increases to an approximately constant value.

To analyze the changes in peak intensity, we fit the scattered peak intensity using Avrami's model by the following equations.

Table 1. Avrami Index and Transformation Rate of bcc and fcc at Different Volume Fractions

	Avrami index (n)		transformation rate ($k^{1/n}$)	
volume fraction (%)	bcc decay	fcc growth	bcc decay	fcc growth
0.75	1.44	1.52	0.066	0.063
0.92	1.46	1.48	0.276	0.266

Then the growth of the fcc phase and the decay of the metastable bcc phase can be described.

$$\text{growth of FCC phase} : I(t) - I(t_0) = [I(t_\infty) - I(t_0)](1 - e^{-k(t-t_0)^n}) \quad (6)$$

$$\text{decay of BCC phase} : I(t) - I(t_\infty) = [I(t_0) - I(t_\infty)]e^{-k(t-t_0)^n} \quad (7)$$

where n is Avrami's index, k is the transformation rate constant, and t_0 is the time at which the transformation from bcc to fcc becomes apparent and it is taken as 9 min for 0.75% and 1.5 min for 0.92% in these analyses. Our experimental data can be perfectly fitted by eqs 6 and 7 as shown in Figure 7, and the values of the Avrami index n and the transformation rate $k^{1/n}$ evaluated from the fitting results are shown in Table 1.

The exponent n is supposed to reflect the geometry of the growing crystal and is associated with the mechanism of crystal growth.[52] Under conditions when all nucleation sites are saturated in the beginning, a relationship, $n = 3 - d$, exists between exponent n and the spatial dimensionality d of the interface on which growth and/or transformation occurred. If growth occurs on the boundary surface between two grains, then $d = 2$ and $n = 1$, whereas if the growth occurs on an edge among three adjacent grains, then $d = 1$ and $n = 2$.

For volume fraction 0.75%, n is 1.44 and 1.52 for the decay of bcc and the growth of fcc, respectively. The Avrami indices are approximately the same, which indicate that the mechanisms of bcc decay and fcc growth are the same, as expected for a transformation process. The same conclusion can also be found for the sample with a volume fraction of 0.92%, where the Avrami index n is 1.46 and 1.48. We can further conclude that the values of n are basically the same for the two volume fractions; that is, the volume fraction has little influence on the transformation mechanism. The average Avrami index n is about 1.48, which lies between the values predicted for grain boundary nucleation and grain edge nucleation after saturation. Commonly, in homogeneous nucleation n is an integer and a noninteger value of n is usually associated with heterogeneous nucleation.

For each volume fraction, Table 1 shows that the transformation rate $k^{1/n}$ of bcc decay is close to that of fcc growth. This also supports the conclusion that the mechanism of bcc decay and fcc growth is the same for a given volume fraction. However, when the volume fraction increases from 0.75 to 0.92%, we find that the transformation rate increases about 4-fold. This implies that the transformation process is faster for larger volume fractions. Such a difference can also be directly reflected in Figures 3 and 4, in which we can see that the time range needed for complete transition is shorter for 0.92% (about 8 min) than that for 0.75% (about 30 min). In atomic and molecular system, as is well

dx.doi.org/10.1021/la200407h |*Langmuir* 2011, 27, 7439–7445

known, supersaturation is the driving force of the crystallization and the rate of nucleation and growth is controlled by the existing supersaturation level in the solution. For a colloidal model system, the volume fraction may be analogous to the role played by supersaturation to some extent. For larger volume fractions, the supersaturation is higher so that the crystallization and transformation from bcc to fcc is faster.

CONCLUSIONS

In this article, by treating the data from the reflection spectrum, we present an investigation on changing trends in a set of parameters characterizing the crystallization process during the disorder−bcc−fcc transition. These parameters include the crystallinity, the average crystal size, the number density of the crystallites, the lattice constant, and the shortest interparticle distance for both bcc and fcc structures. The experimental results show that both the crystallinity and size of the bcc structure keep decreasing during the bcc−fcc transformation and the number of crystallites increases a little and then decreases. For fcc, the crystallinity and size keep increasing during the transformation. The number of crystallites with fcc structure decreases quickly in the early stage of the transformation and basically maintains a constant value in the later stages of the transformation. However, values of the lattice constant and interparticle distance remain almost invariable for both bcc and fcc structures. In addition, the evolution trends in bcc decay and fcc growth are quantitatively analyzed by Avrami's model for two different volume fractions. On the basis of the above investigations, associated kinetic features of the crystallization with the disorder−bcc−fcc transition can be summarized below.

(1) From the time-dependent changes of some structural parameters including crystallinity and the average crystal size, a possible transformation path is sketched. Cleavage of the metastable bcc grains and coalescence of the fcc grains may exist in the transition process.

(2) The Avrami index is similar for the decay of bcc and the growth of fcc, which indicates that the same mechanism is used in bcc decay and fcc growth. This result is further supported by the similarity of the transformation rate. The average Avrami index obtained in our experiments lies between the values predicted for grain boundary nucleation and grain edge nucleation. The results indicate that heterogeneous nucleation exists in the transformation.

(3) The transformation rates for two volume fractions are calculated using Avrami's model. The results show that the transformation rate increases about 4-fold when the volume fraction increases from 0.75 to 0.92%, though it has little influence on the Avrami index. Here, apparently, similar to supersaturation in atomic and molecular systems, as the thermodynamic driving force of phase transition, a larger volume fraction in the colloidal system can accelerate the crystallization and relevant transformation process. However, the small influence of volume fraction on the Avrami index indicates that the transformation mechanisms for different volume fractions are basically the same.

AUTHOR INFORMATION

Corresponding Author

*Tel: +86 10 82544093. Fax: +86 10 82544096. E-mail: sunzw@imech.ac.cn.

ACKNOWLEDGMENT

This work was supported by the National Natural Science Foundation of China (grant nos. 10972217 and 11032011), the Knowledge Innovation Program of the Chinese Academy of Sciences (grant no. KJCX2-YW-L08), and the National Science Foundation for Postdoctoral Scientists of China (grant no. 20100480482).

REFERENCES

(1) Gasser, U. *J. Phys.: Condens. Matter* **2009**, *21*, 203101.
(2) Yethiraj, A.; van Blaaderen, A. *Nature* **2003**, *421*, 513–517.
(3) Tata, B. V. R.; Jena, S. S. *Solid State Commun.* **2006**, *139*, 562–580.
(4) Ise, N.; Konishi, T.; Tata, B. V. R. *Langmuir* **1999**, *15*, 4176–4184.
(5) Palberg, T. *Curr. Opin. Colloid Interface Sci.* **1997**, *2*, 607–614.
(6) Palberg, T. *J. Phys.: Condens. Matter* **1999**, *11*, R323–R360.
(7) Okubo, T. *Acc. Chem. Res.* **1988**, *21*, 281–286.
(8) Gast, A. P.; Russel, W. B. *Phys. Today* **1998**, *51*, 24–30.
(9) Ise, N.; Sogami, I. S. *Structure Formation in Solution: Ion Polymers and Colloidal Particles*: Springer, 2005.
(10) Alexander, S.; McTague, J. *Phys. Rev. Lett.* **1978**, *41*, 702–705.
(11) Anderson, V. J.; Lekkerkerker, H. N. W. *Nature* **2002**, *416*, 811–815.
(12) Schöpe, H. J.; Decker, T.; Palberg, T. *J. Chem. Phys.* **1998**, *109*, 10068–10074.
(13) Desgranges, C.; Delhommelle, J. *Phys. Rev. Lett.* **2007**, *98*, 235502.
(14) Shen, Y. C.; Oxtoby, D. W. *Phys. Rev. Lett.* **1996**, *77*, 3585–3588.
(15) Gu, L. Y.; Xu, S. H.; Sun, Z. W.; Wang, J. T. *J. Colloid Interface Sci.* **2010**, *350*, 409–416.
(16) Xu, S.; Zhou, H.; Sun, Z.; Xie, J. *Phys. Rev. E* **2010**, *82*, 010401.
(17) Iacopini, S.; Palberg, T.; Schöpe, H. J. *J. Chem. Phys.* **2009**, *130*, 084502.
(18) Wette, P.; Engelbrecht, A.; Salh, R.; Klassen, I.; Menke, D.; Herlach, D. M.; Roth, S. V.; Schöpe, H. J. *J Phys.: Condens. Matter* **2009**, *21*, 464115.
(19) Schöpe, H. J.; Bryant, G.; van Megen, W. *J. Chem. Phys.* **2007**, *127*, 084505.
(20) Schöpe, H. J.; Bryant, G.; van Megen, W. *Phys. Rev. Lett.* **2006**, *96*, 175701.
(21) Wilding, M. C.; Wilson, M.; McMillan, P. F. *Chem. Soc. Rev.* **2006**, *35*, 964–986.
(22) Kitamura, M. *J. Cryst. Growth* **2002**, *237*, 2205–2214.
(23) Notthoff, C.; Feuerbacher, B.; Franz, H.; Herlach, D. M.; Holland-Moritz, D. *Phys. Rev. Lett.* **2001**, *86*, 1038–1041.
(24) Rajamathi, M.; Kamath, P. V.; Seshadri, R. *J. Mater. Chem.* **2000**, *10*, 503–506.
(25) Montanari, E.; Righi, L.; Calestani, G.; Migliori, A.; Gilioli, E.; Bolzoni, F. *Chem. Mater.* **2005**, *17*, 1765–1773.
(26) Heutz, S.; Bayliss, S. M.; Middleton, R. L.; Rumbles, G.; Jones, T. S. *J. Phys. Chem. B* **2000**, *104*, 7124–7129.
(27) Yamada, Y.; Hamaya, N.; Axe, J. D.; Shapiro, S. M. *Phys. Rev. Lett.* **1984**, *53*, 1665–1668.
(28) Machon, D.; Daniel, M.; Pischedda, V.; Daniele, S.; Bouvier, P.; Le Floch, S. *Phys. Rev. B* **2010**, *82*, 140102.
(29) Okubo, T.; Ishiki, H. *J. Colloid Interface Sci.* **2000**, *228*, 151–156.
(30) Okubo, T.; Kimura, H.; Hatta, T.; Kawai, T. *Phys. Chem. Chem. Phys.* **2002**, *4*, 2260–2263.
(31) Okubo, T.; Kimura, H.; Kawai, T.; Niimi, H. *Langmuir* **2003**, *79*, 6014–6018.
(32) Shouldice, G. T. D.; Vandezande, G. A.; Rudin, A. *Eur. Polym. J.* **1994**, *30*, 179–183.
(33) Zhou, H.; Xu, S.; Sun, Z.; Du, X.; Xie, J. *Colloids Surf., A* **2011**, *375*, 50–54.

(34) Mohanty, P. S.; Tata, B. V. R.; Toyotama, A.; Sawada, T. *Langmuir* **2005**, *21*, 11678–11683.
(35) Yoshida, H.; Yamanaka, J.; Koga, T.; Koga, T.; Ise, N.; Hashimoto, T. *Langmuir* **1999**, *15*, 2684–2702.
(36) Konishi, T.; Ise, N.; Matsuoka, H.; Yamaoka, H.; Sogami, I. S.; Yoshiyama, T. *Phys. Rev. B* **1995**, *51*, 3914–3917.
(37) Yamanaka, J.; Yoshida, H.; Koga, T.; Ise, N.; Hashimoto, T. *Langmuir* **1999**, *15*, 4198–4202.
(38) Harland, J. L.; van Megen, W. *Phys. Rev. E* **1997**, *55*, 3054–3067.
(39) Harland, J. L.; Henderson, S. I.; Underwood, S. M.; van Megen, W. *Phys. Rev. Lett.* **1995**, *75*, 3572–3575.
(40) Cheng, Z.; Zhu, J.; Russel, W. B.; Meyer, W. V.; Chaikin, P. M. *Appl. Opt.* **2001**, *40*, 4146–4151.
(41) (a) Avrami, M. *J. Chem. Phys.* **1939**, *7*, 1103–1112. (b) Avrami, M. *J. Chem. Phys.* **1940**, *8*, 212–224. (c) Avrami, M. *J. Chem. Phys.* **1941**, *9*, 177–184.
(42) Kolmogorov, A. N. *Bull. Acad. Sci. USSR, Phys. Ser.* **1937**, *1*, 355–359.
(43) Johnson, W. A.; Mehl, P. A. *Tech. Publ. — Am. Inst. Min. Metall. Eng.* **1939**, *135*, 416–458.
(44) Clavaguera-Mora, M. T.; Clavaguera, N.; Crespo, D.; Pradell, T. *Prog. Mater Sci.* **2002**, *47*, 559–619.
(45) Lee, J. K.; Choi, G.; Kim, D. H.; Kim, W. T. *Appl. Phys. Lett.* **2000**, *77*, 978–980.
(46) Jiang, J. Z.; Zhuang, Y. X.; Rasmussen, H.; Saida, J.; Inoue, A. *Phys. Rev. B* **2001**, *64*, 094208.
(47) Lorenzo, A. T.; Arnal, M. L.; Albuerne, J.; Muller, A. J. *Polym. Test.* **2007**, *26*, 222–231.
(48) Causin, V.; Marega, C.; Marigo, A.; Valentini, L.; Kenny, J. M. *Macromolecules* **2005**, *38*, 409–415.
(49) Liu, S. L.; Chung, T. S. *Polymer* **2000**, *41*, 2781–2793.
(50) Ramos, R. A.; Rikvold, P. A.; Novotny, M. A. *Phys. Rev. B* **1999**, *59*, 9053–9069.
(51) Liu, Y. S.; Nie, H. F.; Bansil, R.; Steinhart, M.; Bang, J.; Lodge, T. P. *Phys. Rev. E* **2006**, *73*, 061803.
(52) Toro-Vazquez, J.; Dibildox-Alvarado, E.; Charó-Alonso, M.; Herrera-Coronado, V.; Gómez-Aldapa, C. *J. Am. Oil. Chem. Soc.* **2002**, *79*, 855–866.

■ NOTE ADDED AFTER ASAP PUBLICATION

This article was published ASAP on May 20, 2011. Changes were made to equation 7. The corrected version was posted on May 25, 2011.